SCIENTIFIC REPORTS

OPEN

SUBJECT AREAS:
ELECTRONIC DEVICES
SOLID-STATE CHEMISTRY

Received
5 September 2014

Accepted
16 December 2014

Published
20 January 2015

Correspondence and requests for materials should be addressed to Y.S. (shimak@scl.kyoto-u.ac.jp)

Strain-induced significant increase in metal-insulator transition temperature in oxygen-deficient Fe oxide epitaxial thin films

Kei Hirai[1], Daisuke Kan[1], Noriya Ichikawa[1], Ko Mibu[2], Yoshitaka Yoda[3], Marina Andreeva[4] & Yuichi Shimakawa[1,5]

[1]Institute for Chemical Research, Kyoto University, Uji, Kyoto 611-0011, Japan, [2]Nagoya Institute of Technology, Nagoya, Aichi 466-8555, Japan, [3]Japan Synchrotron Radiation Research Institute, 1-1-1 Kouto, Sayo-cho, Sayo-gun, Hyogo 679-5198, Japan, [4]Faculty of Physics, M. V. Lomonosov Moscow State University, 119991, Moscow, Russia, [5]Japan Science and Technology Agency, CREST, Uji, Kyoto 611-0011, Japan.

Oxygen coordination of transition metals is a key for functional properties of transition-metal oxides, because hybridization of transition-metal *d* and oxygen *p* orbitals determines correlations between charges, spins and lattices. Strain often modifies the oxygen coordination environment and affects such correlations in the oxides, resulting in the emergence of unusual properties and, in some cases, fascinating behaviors. While these strain effects have been studied in many of the fully-oxygenated oxides, such as ABO_3 perovskites, those in oxygen-deficient oxides consisting of various oxygen coordination environments like tetrahedra and pyramids as well as octahedra remain unexplored. Here we report on the discovery of a strain-induced significant increase, by 550 K, in the metal-insulator transition temperature of an oxygen-deficient Fe oxide epitaxial thin film. The observed transition at 620 K is ascribed to charge disproportionation of $Fe^{3.66+}$ into Fe^{4+} and Fe^{3+}, associated with oxygen-vacancy ordering. The significant increase in the metal-insulator transition temperature, from 70 K in the bulk material, demonstrates that epitaxial growth of oxygen-deficient oxides under substrate-induced strain is a promising route for exploring novel functionality.

Transition-metal oxide epitaxial thin films, which often exhibit behaviors different from those of the bulk oxide, have attracted a great deal of attention as a fascinating platform for exploring novel functionalities[1–5]. This is in part because strong correlations between charges, spins and lattices determine the functional properties of the films, and these correlations are affected by structural distortions from substrate-induced strain effects[6–9]. For thin films of perovskite oxides ABO_3 consisting of corner-shared oxygen octahedra BO_6, such effects result in octahedral distortions including deformations, tilts, and rotations, which are essentially characterized by displacements of the oxygen atoms in the film's lattice[10]. While substrate-induced distortions have been closely correlated with the functional properties of fully oxygenated perovskite oxide thin films, little is known about their effects on thin films of oxygen-deficient perovskites. The oxygen deficiency introduced in the perovskite structure produces various oxygen coordination environments for the transition metals, like tetrahedra and pyramids as well as octahedra[11–13]. Therefore, substrate-induced modifications of such various oxygen coordination units would provide additional routes to controlling the strong correlations and consequently to modifying or even enhancing the functional properties.

We here focus on oxygen-deficient Fe-based perovskite oxides, $SrFeO_x$ (SFO*x*), which exhibit a variety of structural and physical properties depending on their oxygen vacancy concentration[11,14–23]. The general formula of the known phases is described as $SrFeO_{3-1/n}$ with $n = \infty$, 8, 4, 2 and 1. The $n = \infty$ member, $SrFeO_3$, has the simple cubic perovskite structure with corner-shared FeO_6 octahedra and exhibits metallic conduction down to low temperatures[14,15,24–29]. The oxygen vacancies introduced in the $SrFeO_3$ lattice result in the formation of various Fe environments which consist of ordered arrangements of corner-shared oxygen polyhedra including the FeO_4 tetrahedra and FeO_5 pyramids. An important consequence of these ordered arrangements of the oxygen vacancy is a charge-ordering of Fe with different valence states, which impacts on physical properties. In the $n = 8$

member $SrFeO_{2.875}$, with nominal $Fe^{3.75+}$, the oxygen vacancies order at 523 K and the ordering stabilizes the charge-ordered tetragonal phase with $Fe^{4+}O_6$ octahedra, distorted $Fe^{3.5+}O_6$ octahedra, and $Fe^{4+}O_5$ pyramids[11,16]. The tetragonal phase undergoes another phase transition at ~70 K, which is due to charge disproportionation of $Fe^{3.5+}$ into Fe^{4+} and Fe^{3+} and which is accompanied by an abrupt increase in the electrical resistivity[14,27,30,31]. Further increase in the oxygen vacancy concentration leads to $SrFeO_{2.75}$ ($n = 4$) with nominal $Fe^{3.5+}$[11,16,32] and $SrFeO_{2.5}$ ($n = 2$) with nominal Fe^{3+}[16,17,33–38]. Although the oxygen vacancies in $SrFeO_{2.75}$ are ordered at 598 K and those in $SrFeO_{2.5}$ are ordered at 1103 K, charge disproportionation does not occur in these phases.

In this study we discovered in an oxygen-deficient $SrFeO_x$ ($x \sim 2.8$) epitaxial thin film a transport behavior markedly different from the corresponding behavior in the bulk material. The present thin film under substrate-induced tensile strain shows a metal-insulator transition, associated with the charge disproportionation of $Fe^{3.66+}$ into Fe^{4+} and Fe^{3+} at 620 K. This transition temperature is much higher than ~70 K reported for the transition in the bulk material and is also much higher than room temperature. We also found the transition to be accompanied by oxygen-vacancy ordering. This significant increase in the metal-insulator transition temperature demonstrates that epitaxial growth of oxygen-deficient oxides under substrate-induced strain is a promising route for exploring novel functionality.

Results

Preparation of $SrFeO_{2.8}$ epitaxial thin film. A brownmillerite-structure $SrFeO_{2.5}$ (SFO2.5) epitaxial thin film was first prepared on a (001) $SrTiO_3$ (STO) single-crystal substrate by pulsed laser deposition. An x-ray 2θ-θ profile of that film is shown in Fig. 1a, where we see (101) and (202) reflections of SFO2.5 at slightly lower angles than (001) and (002) reflections of the STO substrate. In the x-ray reciprocal space mapping (RSM) shown in Fig. 1c, we see (206), (484), and (602) reflections whose in-plane positions are the same as that of the STO (204) reflection. These x-ray diffraction results confirm that the deposited SFO2.5 brownmillerite thin film consists of multiple domains with (101) orientation and that the in-plane lattice of the each domain is fixed by the substrate lattice[37].

The deposited SFO2.5 thin film was then oxidized into SFO2.5+δ by the air-annealing at 773 K. Figures 1b and 1d show the x-ray 2θ-θ diffraction profile and RSM of the annealed film. One sees that the diffraction peaks shifted to higher 2θ angle positions and the multiple domain structure disappeared, indicating that the out-of-plane lattice spacing of the oxidized film is smaller than that of the as-deposited film. The decreased lattice size seen after the air annealing strongly suggests oxygen incorporation into the brownmillerite structure. Note that the in-plane lattice of the SFO2.5+δ film is still fixed by the substrate lattice.

The valence state of Fe ions in the oxidized thin film was investigated by Mössbauer spectroscopy. Figure 1e shows a room-temperature ^{57}Fe conversion electron Mössbauer spectrum of the oxidized thin film and the result of the peak fitting. (The fitting results are also summarized in Table I.) No signal due to magnetic ordering was observed. The observed spectrum consists of a singlet with an isomer shift (IS) of 0.04 mm/s (the red line in the figure) and two quadrupole doublets with an IS of 0.12 mm/s (the green) and an IS of 0.35 mm/s (the blue). The observed IS values indicate that the singlet originates from Fe^{4+} and that the doublets with the smaller and larger IS values arise from $Fe^{3.5+}$ and Fe^{3+}, respectively[11,39,40]. The relative abundances of the Fe^{4+}, $Fe^{3.5+}$, and Fe^{3+} components are respectively 56%, 20%, and 24%, giving an average oxidation state for Fe of +3.66 and giving an oxygen content of 2.83. Therefore the thin film obtained by air-annealing the SFO2.5 thin film is identified to be the oxygen-deficient perovskite $SrFeO_{2.8}$ (SFO2.8).

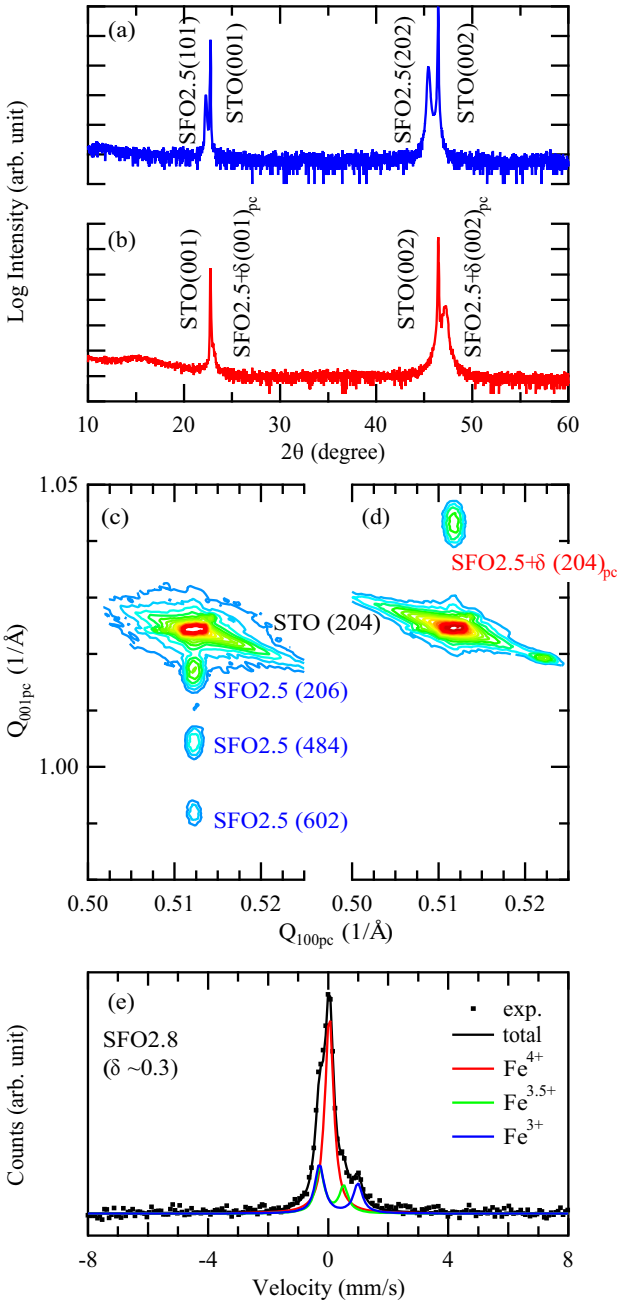

Figure 1 | (a, b) X-ray 2θ-θ profiles for (a) as-deposited brownmillerite $SrFeO_{2.5}$ (SFO2.5) film and (b) oxidized SFO2.5 (SFO2.5+δ) film grown on the STO substrates. (c, d) X-ray reciprocal space mappings around STO (204) reflections for (c) SFO2.5 and (d) SFO2.5+δ thin films. The intensity is plotted on a semi-logarithmic scale. All the data were obtained at room temperature. (e) ^{57}Fe conversion electron Mössbauer spectrum of the SFO2.5+δ thin film at room temperature. The fitting results, which are listed in Table I, are shown with lines in black (total), red (Fe^{4+} singlet component), green ($Fe^{3.5+}$ doublet component), and blue (Fe^{3+} doublet component). Note that the electric field gradients for the $Fe^{3.5+}$ and Fe^{3+} doublets are oriented along the in-plane direction. The oxygen content of the SFO2.5+δ thin film was estimated to be 2.83.

Metal-insulator transition associated with charge disproportionation above room temperature in $SrFeO_{2.8}$ thin film. In contrast to the bulk SFO2.8, the electrical resistivity of the prepared film is as high as 1 Ωcm at room temperature. The quite high resistivity of the film decreased with increasing temperature and reached ~3 mΩcm at temperatures above 620 K (Fig. 2). We can clearly see that the

Table I | The isomer shift (IS) and the quadrupole splitting (QS) parameters obtained by fitting the ^{57}Fe internal conversion electron Mössbauer spectra of the oxidized SFO2.5 (SFO2.8) thin film at 300 K. The directions of the electric field gradients of the $Fe^{3.5+}$ and Fe^{3+} doublet components are set to be parallel to the in-plane direction of the film

Component	Multiplet	IS (mm/s)	QS (mm/s)	Area (%)
Fe^{4+}	Singlet	0.04	—	56
$Fe^{3.5+}$	Doublet	0.12	0.80	20
Fe^{3+}	Doublet	0.35	1.28	24

metal-insulator transition occurs at 620 K, and this transition suggests a significant change in the valence states of Fe in the film at that temperature. To clarify the nature of transition, we measured the time spectra of the nuclear resonant ("^{57}Fe Mössbauer") scattering[41,42]. The measured spectra of the SFO2.8 film at 300, 573, and 673 K in air are shown in Fig. 3 together with the theoretically simulated spectrum patterns. It is clear that the oscillation patterns in the time spectra are different below and above the transition temperature. The spectrum at 300 K shows time-dependent oscillation, and the oscillation pattern is well reproduced with three components with distinct hyperfine parameters as listed in Table II. The result is in good agreement with that independently obtained in the ^{57}Fe conversion electron Mössbauer measurement shown in Fig. 1e. The time spectrum at 573 K is essentially the same as that at 300 K. The parameters obtained from its analysis (also listed in Table II) confirm that the valence states of Fe in the film and the relative abundance do not change with changes in temperature below the metal-insulator transition temperature and that the thin film below the metal-insulator transition temperature contains Fe^{4+} (55%), $Fe^{3.5+}$ (15%), and Fe^{3+} (30%). Importantly, the relative abundance of each Fe components in the film below the transition temperature is essentially the same as that in the charge-disproportionated insulating phase of bulk SFO2.8[27]. The results indicate that below the transition temperature the most of Fe in the film have the integer valence state of either Fe^{4+} or Fe^{3+} and thus the charge-disproportionated state is formed. This is also consistent with the observed high resistivity of the SFO2.8 thin film.

The spectrum at 673 K (above the transition temperature), on the other hand, shows no oscillation pattern and can well be reproduced by a single component with an IS of –0.04 mm/s. This IS value is quite small, suggesting that the Fe ion in the SFO2.8 thin film at this temperature has an unusually high oxidation state. Given that the oxygen content of the film does not change up to this temperature[16], the result indicates that the film above the metal-insulator transition

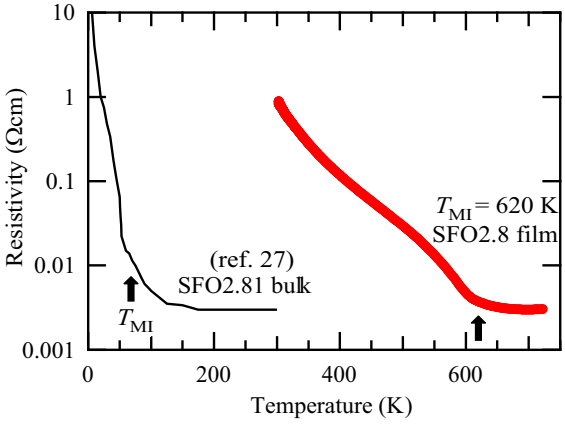

Figure 2 | Temperature dependence of the electrical resistivity of SFO2.8 film from 720 to 300 K in air (red line) and $SrFeO_x$ ($x \approx 2.81$) bulk from 300 to 5 K (black line). The arrows denote the metal-insulator transition temperatures T_{MI}. The resistivity data of the SFO2.81 bulk were taken from a report by P. Adler *et al.* (Ref. 27).

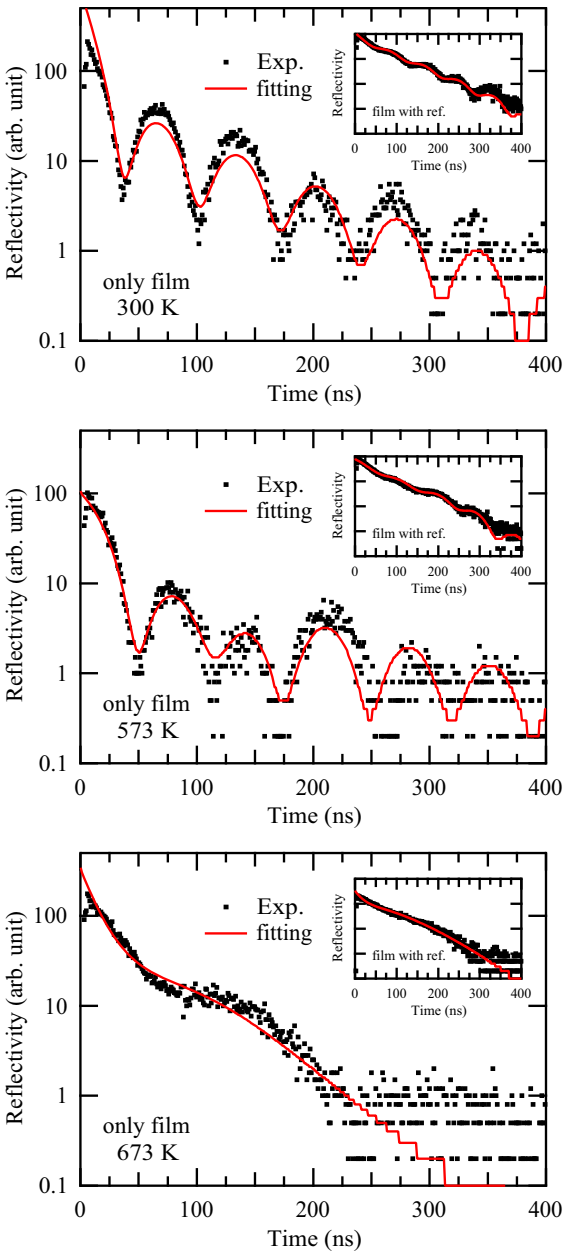

Figure 3 | Time spectra of the nuclear resonant spectra of SFO2.8 thin film at 300, 573 and 673 K in air. The inset in each panel shows the time spectrum of reflectivity taken with the reference $K_2MgFe(CN)_6$ sample. The ISs of the Fe ion components in the film were determined by fitting the inset spectra. Black dots and red lines correspond to the experimental data and fitting results, respectively. The spectra at 300 and 573 K can be reproduced with three components of Fe^{4+}, $Fe^{3.5+}$, and Fe^{3+}. The spectrum at 673 K can be fitted with a single component of $Fe^{3.66+}$. The parameters obtained from the fittings are listed in Table II.

Table II | The isomer shift (IS) and the quadrupole splitting (QS) parameters obtained by fitting the time spectra of the nuclear resonant scattering of the SFO2.8 thin film at 300, 573, and 673 K. The directions of the electric field gradients of the $Fe^{3.5+}$ and Fe^{3+} doublet components are parallel to the in-plane direction of the film

Temperature (K)	Component	Multiplet	IS (mm/s)	QS (mm/s)	Area (%)
300	Fe^{4+}	Singlet	0.01	—	55
	$Fe^{3.5+}$	Doublet	0.13	0.79	15
	Fe^{3+}	Doublet	0.32	1.25	30
573	Fe^{4+}	Singlet	0.00	—	53
	$Fe^{3.5+}$	Doublet	0.10	0.81	14
	Fe^{3+}	Doublet	0.22	1.23	33
673	$Fe^{3.66+}$	Singlet	−0.04	—	100

temperature has a single Fe site with a mixed-valence state of $Fe^{3.66+}$. This single Fe site also suggests that the oxygen vacancies are disordered above the transition temperature[43]. Our analysis of the time spectra of the nuclear resonant scattering therefore leads to a conclusion that the metal-insulator transition seen in the SFO2.8 thin film at 620 K is due to the charge disproportionation of $Fe^{3.66+}$ above the transition temperature into Fe^{4+} and Fe^{3+} below the temperature.

Structural transition due to oxygen-vacancy ordering. We also investigated whether a structural change at the metal-insulator transition temperature occurs in our SFO2.8 thin film. Figure 4 shows temperature dependence of the out-of-plane lattice spacing of the film together with that of the cubic STO substrate, both of which were obtained in the x-ray 2θ-θ measurements at temperatures between 720 and 300 K in air. We found that with decreasing temperature the out-of-plane lattice spacing of the film decreased abruptly at 620 K, where the metal-insulator transition occurred. It is clear that the structural change in the film was not caused by the substrate lattice, which exhibits the normal thermal change. We also confirmed from the RSM measurements that the in-plane lattice of the film (the open red square in Fig. 4) is fixed by the substrate lattice both above and below the transition temperature. The quite large change in the out-of-plane lattice spacing seen at 620 K indicates that the structural transition in our oxygen-deficient SFO2.8 thin film is due to a change in oxygen-vacancy ordering. Thus the charge disproportionation transition in Fe in the SFO2.8 thin film is accompanied by both a metal-insulator transition and an oxygen-ordering structural transition.

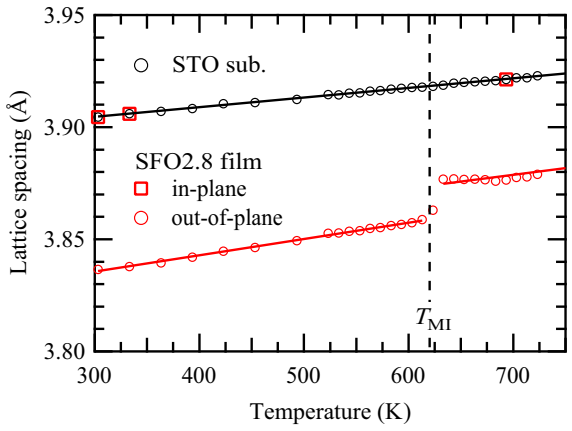

Figure 4 | Temperature dependence of the out-of-plane (circles) and in-plane (squares) lattice spacings for the SFO2.8 film (red) and the STO substrate (black) from 720 K to room temperature in air. The in-plane lattice of the film is fixed by the substrate in the entire range of temperatures. The dashed line denotes the metal-insulator transition temperature T_{MI} (= 620 K) of the SFO2.8 film.

Discussion

The experimental results described above indicate that the present SFO2.8 thin film undergoes not only a structural transition due to oxygen-vacancy ordering at 620 K but also the charge disproportionation of $Fe^{3.66+}$ into Fe^{4+} and Fe^{3+} at that temperature. Similar oxygen-vacancy ordering and charge disproportionation transitions were reported in bulk $SrFeO_x$ ($x \approx 2.8$) samples, but in those samples the oxygen-vacancy ordering occurred at 523–598 K and the charge disproportionation took place around 70 K[16,27]. Interestingly, while the oxygen-vacancy ordering in bulk at 523–598 K is not accompanied by changes in transport properties, the charge disproportionation at 70 K induces a metal-insulator-like resistivity jump. Thus the metal-insulator (and also charge disproportionation) transition temperature of 620 K of the film is significantly higher than the transition temperature reported in the bulk material[27,30]. We note that the oxygen ordering temperature also increases. The behaviors different from those of the bulk samples are likely to be related to the substrate-induced strain effect in our epitaxial thin film.

Assuming that the low-temperature charge-disproportionated phase (< 620 K) of the present thin film is similar to that of the bulk $SrFeO_x$ ($x \approx 2.8$), the oxygen-deficient octahedra $Fe^{3.66+}O_{5.66}$ in the high-temperature phase changes into $Fe^{4+}O_5$ pyramids, $Fe^{4+}O_6$ octahedra, $Fe^{3.5+}O_6$ octahedra, and $Fe^{3+}O_6$ octahedra at the transition temperature of 620 K. Our experimental results indicate that because the SFO2.8 film is subjected to significant tensile strain by the substrate lattice, the stretched film's lattice stabilizes long Fe-O bonds like the Fe^{3+}-O bond. In fact, the average Fe^{3+}-O bond distance observed in the charge-disproportionated bulk sample was much shorter than expected for a typical ionic bond[14]. Thus, the lattice stretched by the tensile strain is preferable for stabilizing the low-temperature $Fe^{3+}O_6$ octahedra, and consequently the charge-disproportionated phase in the film is more stable than the phase in the bulk, leading to the increase in transition temperature.

It is also interesting to point out that the transition temperatures of the charge disproportionation for fully-oxygenated perovskite oxides such as $CaFeO_3$ and $La_{0.33}Sr_{0.67}FeO_3$, unlike the oxygen-deficient perovskite $SrFeO_{2.8}$, are little influenced by substrate-induced strain[44–46]. No significant changes in the charge disproportionation transition temperature were observed when the strained thin films were compared with the bulk materials. This implies that the fully oxygenated octahedral network is pretty rigid, whereas the oxygen-deficient compounds, which contain various oxygen coordination environments, have structural flexibility that lets them accommodate the strain-induced deformation of the polyhedra. Given the diverse oxygen coordination environments seen in oxygen-deficient transition-metal oxides like cobaltites, strain-induced modification of oxygen coordination environments can therefore be useful to improve the functional properties and even to explore novel functionality of oxygen-deficient oxide thin films.

Methods

Preparation of $SrFeO_{2.8}$ thin films. $SrFeO_{2.8}$ (SFO2.8) thin films were prepared by oxidizing brownmillerite-structured $SrFeO_{2.5}$ (SFO2.5) thin films. The SFO2.5 films with thicknesses of 20–100 nm were epitaxially grown on (001) $SrTiO_3$ (STO) single-crystal substrates by pulsed laser deposition. During the thin film deposition, the stoichiometric target was ablated at 2 Hz with a KrF excimer laser ($\lambda = 248$ nm, COHERENT COMPex-Pro 205 F) with a laser spot density of 1 J/cm^2 on the target surface. The oxygen partial pressure and the substrate temperature were kept at 1×10^{-5} Torr and 973 K. The deposited SFO2.5 films were oxidized to SFO2.8 by annealing them in air at 773 K. The oxygen content in the films was evaluated from the relative abundances of Fe^{4+}, $Fe^{3.5+}$, and Fe^{3+} obtained from the fitting of ^{57}Fe internal conversion electron Mössbauer spectrum measured at room temperature.

Structural characterizations. The crystal structures and growth orientations of the as-deposited SFO2.5 thin films and the SFO2.8 films were characterized with a conventional four-circle X-ray diffractometer (PANalytical X'Pert MRD) equipped with a high-temperature sample stage (DHS1100) and operated with Cu $K\alpha_1$ radiation. The indices of the diffraction peaks of SFO2.5 are based on a bulk orthorhombic cell ($a = 5.67$ Å, $b = 15.59$ Å, and $c = 5.53$ Å) and those of SFO2.8 are based on a pseudo-cubic perovskite cell. The out-of-plane lattice spacing of the SFO2.8 film was determined from the (002) Bragg reflection position in a 2θ-θ diffraction pattern, and the in-plane lattice spacing was estimated from the (204) reflection position in the reciprocal space mapping. All diffraction measurements were carried out in air.

Electrical characterizations. Electrical resistivity of the SFO2.8 thin films was measured, in a voltage-source mode, by a two-terminal method. Pt metal electrodes were sputtered at room temperature. The temperature dependence of resistivity was obtained while cooling the samples from 773 K to room temperature in air.

^{57}Fe internal conversion electron Mössbauer measurements. The internal conversion electron Mössbauer spectroscopy measurements with the ^{57}Fe excitation energy, 14.4 keV, were performed to see the valence states of Fe in the SFO2.8 thin films. The source velocity was calibrated by using a pure α-Fe film. A 10 mm × 10 mm SFO2.8 thin film with thickness of 100 nm was used for the measurement. The Mössbauer spectrum was fitted with Lorentzian functions by using the "Fit;o)" program.

Measurements of time spectra of the nuclear resonant scattering. The measurements were conducted in a total reflection geometry (a grazing incidence angle of ~0.3°) at the beam line BL09XU of SPring-8. Incident photons were tuned to the ^{57}Fe Mössbauer resonance at 14.4 keV by using a monochromator with 2.2 meV resolution. An eight-cell avalanche photodiode detector made from a thin silicon wafer with a depletion region of around 60 mm was used. The temperature of the thin-film samples was controlled by a resistive heater, and the spectra were measured at 300, 573, and 673 K in air.

To determine isomer shift (IS) for the Fe ion components in the film from the time spectra, two types of spectra were collected at each measuring temperature. One was measured with only the film. The other was measured with the film and the reference. For the measurement of the latter spectra, a plate of $K_2MgFe(CN)_6$ (RITVERC GmbH) was used as a reference sample and was placed in front of the films during the measurements. The forward scattering time spectrum of the reference sample was also measured separately and its scattering amplitude spectrum was determined by fitting this time spectrum. The obtained nuclear resonance characteristics of the reference were in compliance with initially given parameters: IS = –0.101 mm/s relative to the IS of α-Fe, the line width is 0.165 mm/s, and the ^{57}Fe density 0.25 mg/cm^2.

The theoretical simulations were performed by using the "REFTIM" program package[47], which was modified in order to take into account the existence of the reference sample in the beam in some experiments and was adjusted for calculations of the forward scattering time spectrum as well (for the fit of the spectra for the reference sample). At the beginning the prompt reflectivity curve from the SFO2.8 film on the STO substrate was fitted and the obtained parameters of the electronic density depth distribution were used. These parameters were fixed in the model intended for the fit of the time spectra of the nuclear resonant reflectivity. The exact thickness of the SFO2.8 film was 107.4 nm, and the mean square roughness of the surface was 0.8 nm.

1. Hwang, H. Y. *et al.* Emergent phenomena at oxide interfaces. *Nat. Mater.* **11**, 103–113 (2012).
2. Ohtomo, A. & Hwang, H. Y. A high-mobility electron gas at the $LaAlO_3/SrTiO_3$ heterointerface. *Nature* **427**, 423–426 (2004).
3. Lee, H. N., Christen, H. M., Chisholm, M. F., Rouleau, C. M. & Lowndes, D. H. Strong polarization enhancement in asymmetric three-component ferroelectric superlattices. *Nature* **433**, 395–399 (2005).
4. Bousquet, E. *et al.* Improper ferroelectricity in perovskite oxide artificial superlattices. *Nature* **452**, 732–736 (2008).
5. Boris, A. V. *et al.* Dimensionality control of electronic phase transitions in nickel-oxide superlattices. *Science* **332**, 937–940 (2011).
6. Locquet, J.-P. *et al.* Doubling the critical temperature of $La_{1.9}Sr_{0.1}CuO_4$ using epitaxial strain. *Nature* **394**, 453–456 (1998).
7. Choi, K. J. *et al.* Enhancement of ferroelectricity in strained $BaTiO_3$ thin films. *Science* **306**, 1005–1009 (2004).
8. Haeni, J. H. *et al.* Room-temperature ferroelectricity in strained $SrTiO_3$. *Nature* **430**, 758–761 (2004).
9. Lee, J. H. *et al.* A strong ferroelectric ferromagnet created by means of spin-lattice coupling. *Nature* **466**, 954–958 (2010).
10. Aso, R., Kan, D., Shimakawa, Y. & Kurata, H. Atomic level observation of octahedral distortions at the perovskite oxide heterointerface. *Sci. Rep.* **3**, 2214 (2013).
11. Hodges, J. P. *et al.* Evolution of oxygen-vacancy ordered crystal structures in the perovskite series $Sr_nFe_nO_{3n-1}$ ($n = 2$, 4, 8, and ∞), and the relationship to electronic and magnetic properties. *J. Solid State Chem.* **151**, 190–209 (2000).
12. Chernov, S. V. *et al.* Sr_2GaScO_5, $Sr_{10}Ga_6Sc_4O_{25}$, and $SrGa_{0.75}Sc_{0.25}O_{2.5}$: a play in the octahedra to tetrahedra ratio in oxygen-deficient perovskites. *Inorg. Chem.* **51**, 1094–1103 (2012).
13. Poeppelmeier, K. R., Leonowicz, M. E. & Longo, J. M. $CaMnO_{2.5}$ and $Ca_2MnO_{3.5}$: New oxygen-defect perovskite-type oxides. *J. Solid State Chem.* **44**, 89–98 (1982).
14. Reehuis, M. *et al.* Neutron diffraction study of spin and charge ordering in $SrFeO_{3-\delta}$. *Phys. Rev. B* **85**, 184109 (2012).
15. MacChesney, J. B., Sherwood, R. C. & Potter, J. F. Electric and magnetic properties of the strontium ferrates. *J. Chem. Phys.* **43**, 1907–1913 (1965).
16. Takeda, Y. *et al.* Phase relation in the oxygen nonstoichiometric system, $SrFeO_x$ ($2.5 \leq x \leq 3.0$). *J. Solid State Chem.* **63**, 237–249 (1986).
17. D'Hondt, H. *et al.* Tetrahedral chain order in the $Sr_2Fe_2O_5$ brownmillerite. *Chem. Mater.* **20**, 7188–7194 (2008).
18. Williams, G. V. M., Hemery, E. K. & McCann, D. Magnetic and transport properties of $SrFeO_x$. *Phys. Rev. B* **79**, 024412 (2009).
19. Peets, D. C., Kim, J., Reehuis, M., Dosanjh, P. & Keimer, B. Floating zone growth of large single crystals of $SrFeO_{3-\delta}$. *J. Cryst. Growth* **361**, 201–205 (2012).
20. Tsujimoto, Y. *et al.* Infinite-layer iron oxide with a square-planar coordination. *Nature* **450**, 1062–1065 (2007).
21. Inoue, S. *et al.* Single-crystal epitaxial thin films of $SrFeO_2$ with FeO_2 'infinite layers'. *Appl. Phys. Lett.* **92**, 161911 (2008).
22. Kawakami, T. *et al.* Spin transition in a four-coordinate iron oxide. *Nat. Chem.* **1**, 371–376 (2009).
23. Matsumoto, K. *et al.* Oxygen incorporation into infinite-layer structure $AFeO_2$ (A = Sr or Ca). *Chem. Lett.* **42**, 732–734 (2013).
24. Takeda, T., Yamaguchi, Y. & Watanabe, H. Magnetic structure of $SrFeO_3$. *J. Phys. Soc. Jpn.* **33**, 967–969 (1972).
25. Bocquet, A. E. *et al.* Electronic structure of $SrFe^{4+}O_3$ and related Fe perovskite oxides. *Phys. Rev. B* **45**, 1561–1570 (1992).
26. Yamada, H., Kawasaki, M. & Tokura, Y. Epitaxial growth and valence control of strained perovskite $SrFeO_3$ films. *Appl. Phys. Lett.* **80**, 622–624 (2002).
27. Adler, P. *et al.* Magnetoresistance effects in $SrFeO_{3-\delta}$: Dependence on phase composition and relation to magnetic and charge order. *Phys. Rev. B* **73**, 094451 (2006).
28. Solís, C. *et al.* Microstructure and high temperature transport properties of high quality epitaxial $SrFeO_{3-\delta}$ films. *Solid State Ion.* **179**, 1996–1999 (2008).
29. Ishiwata, S. *et al.* Versatile helimagnetic phases under magnetic fields in cubic perovskite $SrFeO_3$. *Phys. Rev. B* **84**, 054427 (2011).
30. Lebon, A. *et al.* Magnetism, charge order, and giant magnetoresistance in $SrFeO_{3-\delta}$ single crystals. *Phys. Rev. Lett.* **92**, 037202 (2004).
31. Hemery, E. K., Williams, G. V. M. & Trodahl, H. J. Anomalous thermoelectric power in $SrFeO_{3-\delta}$ from charge ordering and phase separation. *Phys. Rev. B* **75**, 092403 (2007).
32. Schmidt, M., Hofmann, M. & Campbell, S. J. Magnetic structure of strontium ferrite $Sr_4Fe_4O_{11}$. *J. Phys. Condens. Matter* **15**, 8691–8701 (2003).
33. Schmidt, M. & Campbell, S. J. Crystal and magnetic structures of $Sr_2Fe_2O_5$ at elevated temperature. *J. Solid State Chem.* **156**, 292–304 (2001).
34. Paulus, W. *et al.* Lattice dynamics to trigger low temperature oxygen mobility in solid oxide ion conductors. *J. Am. Chem. Soc.* **130**, 16080–16085 (2008).
35. Chakraverty, S., Ohtomo, A., Okude, M., Ueno, K. & Kawasaki, M. Epitaxial structure of (001)- and (111)-oriented perovskite ferrate films grown by pulsed-laser deposition. *Cryst. Growth Des.* **10**, 1725–1729 (2010).
36. Hirai, K., Kan, D., Ichikawa, N. & Shimakawa, Y. Epitaxial growth of brownmillerite-structure $Sr_{1-x}La_xFeO_{2.5}$ thin films. *Proc. Powder Metall. World Congr.* 16F-T14-18, 1–6 (2012).
37. Hirai, K. *et al.* Anisotropic in-plane lattice strain relaxation in brownmillerite $SrFeO_{2.5}$ epitaxial thin films. *J. Appl. Phys.* **114**, 053514 (2013).
38. Auckett, J. E. *et al.* Combined experimental and computational study of oxide ion conduction dynamics in $Sr_2Fe_2O_5$ brownmillerite. *Chem. Mater.* **25**, 3080–3087 (2013).
39. Li, X. *et al.* Mössbauer spectroscopic study on nanocrystalline $LaFeO_3$ materials. *Hyperfine Interact.* **69**, 851–854 (1992).
40. Blaauw, C. & Woude, F. van der. Magnetic and structural properties of $BiFeO_3$. *J. Phys. C Solid State Phys.* **6**, 1422–1431 (1973).
41. Röhlsberger, R. *Nuclear Condensed Matter Physics with Synchrotron Radiation: Basic Principles, Methodology and Applications (Springer Tracts in Modern Physics).* **208**, (Springer-Verlag 2004).
42. Röhlsberger, R. Nuclear resonant scattering of synchrotron radiation from thin films. *Hyperfine Interact.* **123-124**, 455–479 (1999).

43. Takano, M. *et al.* Dependence of the structure and electronic state of $SrFeO_x$ ($2.5 \leq x \leq 3$) on composition and temperature. *J. Solid State Chem.* **73**, 140–150 (1988).
44. Hayashi, N., Terashima, T. & Takano, M. Oxygen-holes creating different electronic phases in Fe^{4+}-oxides: successful growth of single crystalline films of $SrFeO_3$ and related perovskites at low oxygen pressure. *J. Mater. Chem.* **11**, 2235–2237 (2001).
45. Wadati, H. *et al.* Hole-doping-induced changes in the electronic structure of $La_{1-x}Sr_xFeO_3$: Soft x-ray photoemission and absorption study of epitaxial thin films. *Phys. Rev. B* **71**, 035108 (2005).
46. Okamoto, J. *et al.* Quasi-two-dimensional *d*-spin and *p*-hole ordering in the three-dimensional perovskite $La_{1/3}Sr_{2/3}FeO_3$. *Phys. Rev. B* **82**, 132402 (2010).
47. Andreeva, M. A. Nuclear resonant reflectivity data evaluation with the 'REFTIM' program. *Hyperfine Interact.* **185**, 17–21 (2008).

Acknowledgments

This work was partially supported by Grants-in-Aid for Scientific Research (Grants No. 24760009 and 24540346), and a grant for the Joint Project of Chemical Synthesis Core Research Institutions from the Ministry of Education, Culture, Sports, Science and Technology (MEXT) of Japan. The work was also supported by Japan Science and Technology Agency, CREST. The conversion electron ^{57}Fe Mössbauer experiments were supported by the Nanotechnology Platform Project, MEXT, Japan. The experiments at SPring-8 were performed with the approval of the Japan Synchrotron Radiation Research Institute (2013A1184).

Author contributions

K.H., D.K. and Y.S. conceived and designed the project. K.H., D.K. and N.I. prepared the sample and performed structural and transport characterizations. K.M. contributed to the ^{57}Fe internal conversion electron Mössbauer spectroscopy measurement. The time spectra of the nuclear resonant scattering were taken by K.H., D.K. and Y.Y. and were analyzed by K.H. with the help of M.A. Y.S. supervised the project. All of the authors contributed to the interpretation and discussion of the experimental results, and co-wrote the manuscript.

Additional information

Competing financial interests: The authors declare no competing financial interests.

How to cite this article: Hirai, K. *et al.* Strain-induced significant increase in metal-insulator transition temperature in oxygen-deficient Fe oxide epitaxial thin films. *Sci. Rep.* **5**, 7894; DOI:10.1038/srep07894 (2015).